Supplementary Material

for

Mapping Dielectrophoretic and Electrochemical Impedance Spectrum of Metastasis in Breast Cancer Cells via Inkjet Printed Castellated Arrays

Mohamad Fawzi Awad[a‡], Zeina Habli[a‡], Sahera Saleh[a], Marwan El-Sabban[b], Massoud L. Khraiche[a*]

[a] Neural Engineering and Nanobiosensors Group, Biomedical Engineering Program, Maroun Semaan Faculty of Engineering and Architecture, American University of Beirut, Beirut 1107 2020, Lebanon.

[b] Department of Anatomy, Cell Biology, and Physiological Sciences, Faculty of Medicine, American University of Beirut, Beirut 1107 2020, Lebanon.

‡ Equally contributed to work

* Corresponding authors: e-mail address: mkhraiche@aub.edu.lb

S1)

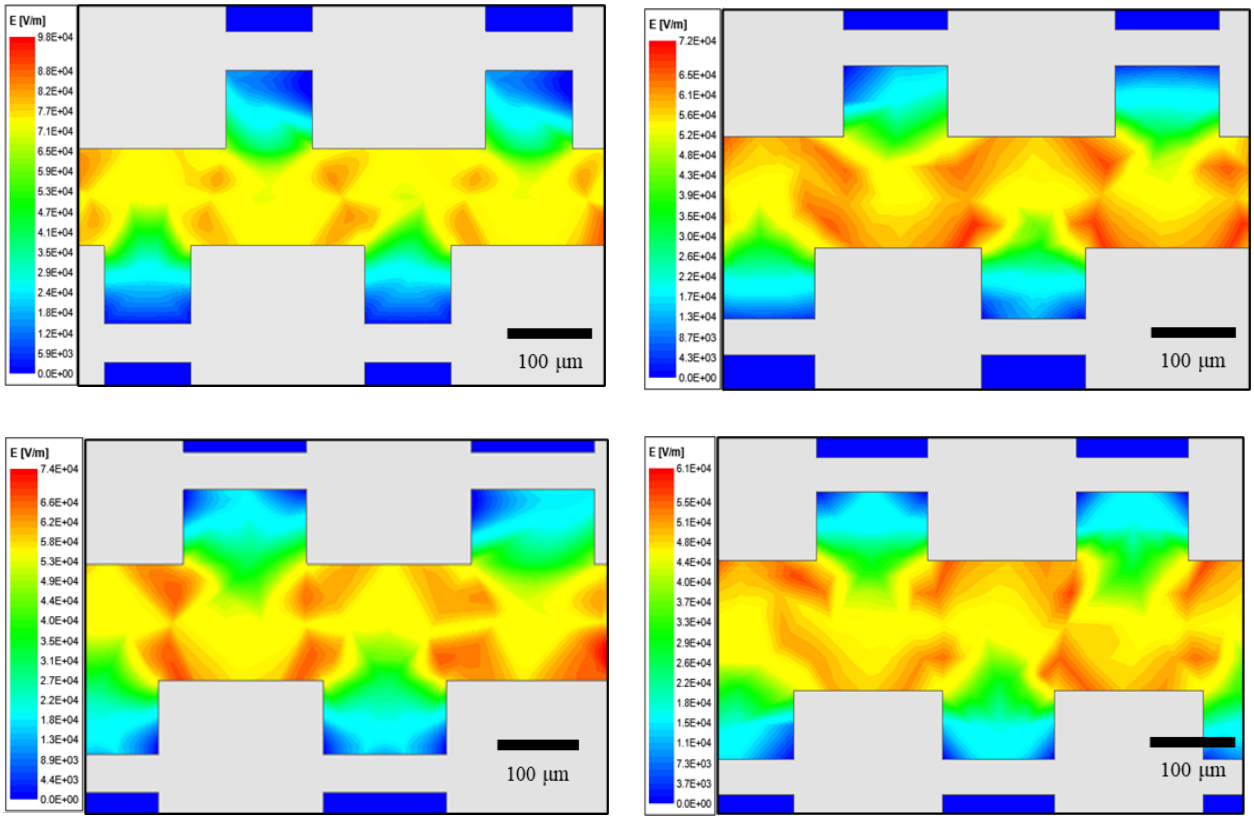

Figure-S1. Simulation of the interdigitated castellated array design with an applied voltage of 4V and varying geometric gaps. The H x V (horizontal x vertical) gaps are as follows: 100x100 µm (top-left), 120x120 µm (top-right), 120x150 µm (bottom-left), 150x150 µm (bottom-right).

S2)

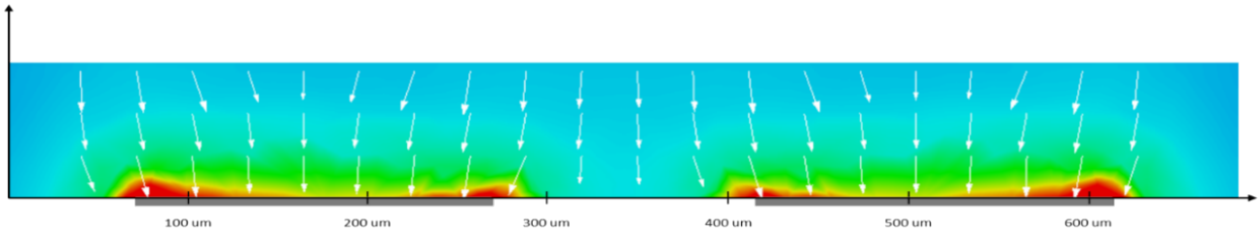

Figure-S2. Visualization of particle dynamics within the spatially-varying, non-uniform electrical field induced by the interdigitated castellated array.

S3)

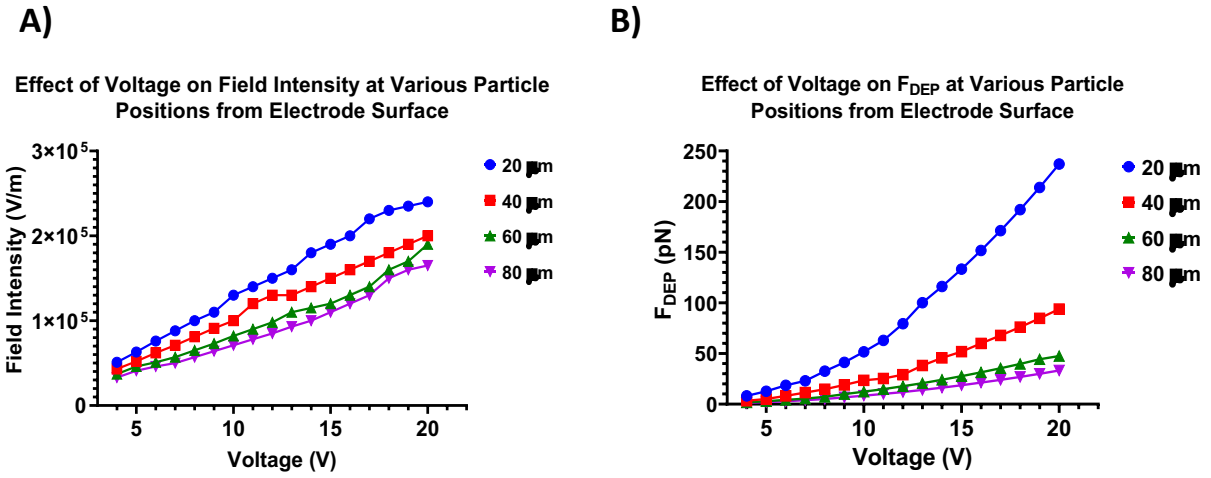

Figure-S3. A) Investigation of the DEP force acting on a 10 µm particle at different vertical positions (z-displacement) under varying voltage conditions. B) Analysis of how changes in voltage and vertical position (z-displacement) influence the gradient of electric field intensity.

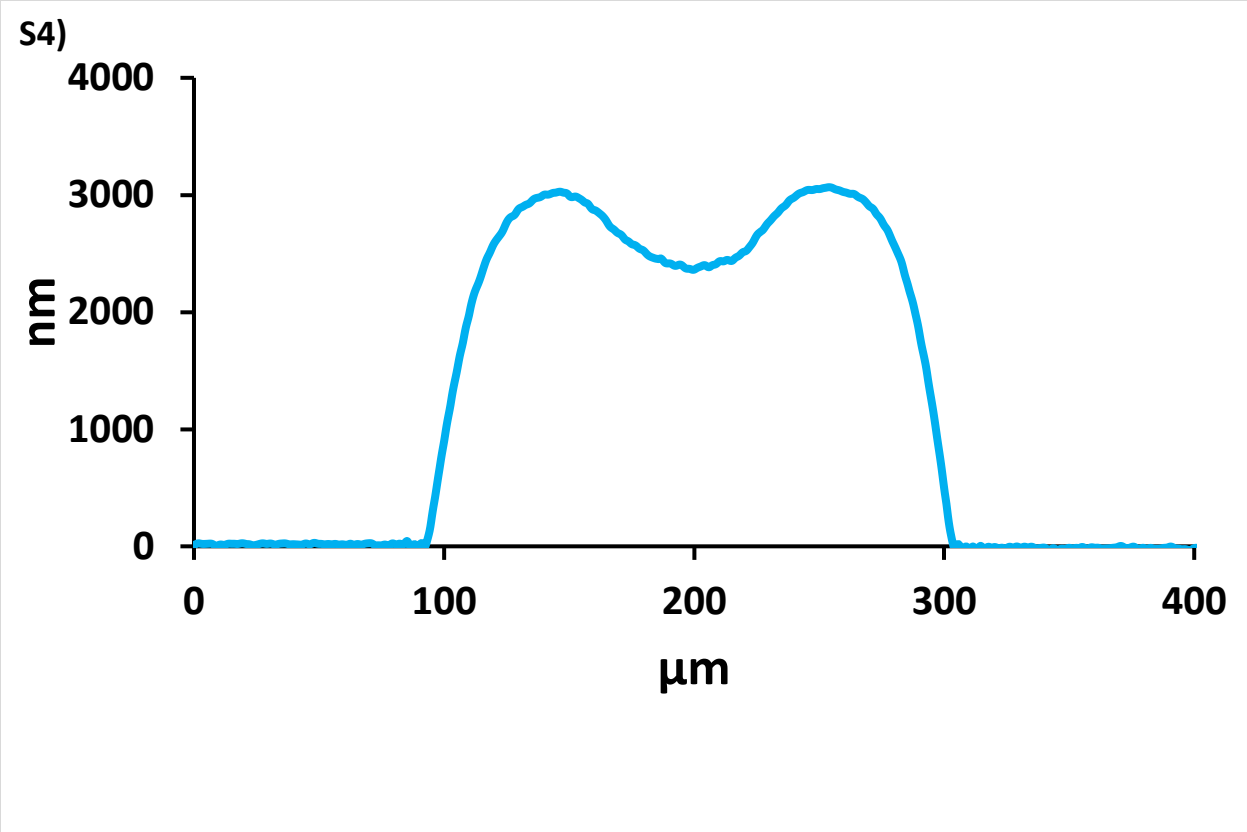

Figure-S4. Averaged cross-sectional profile of a single castellation within the electrode array using DHM profilometry (3 printed layers).

S5)

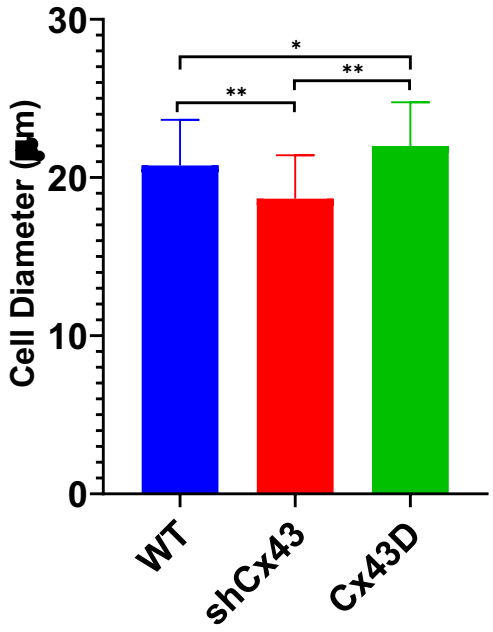

Figure-S5. Comparison of cell radii among MDA-MB-231 cell variants three: wild-type (WT), cells with suppressed Connexin-43 expression (shCx43), and cells with overexpressed Connexin-43 (Cx43D). One-way ANOVA test was performed with significance reported as *, **, and *** when p-value ≤ 0.033, ≤0.002, and ≤0.001, respectively.

Stability of the IJP Devices Post DEP Applications

To evaluate the robustness of the IJP silver electrodes, we assessed the effects of long-term voltage applications on our configured IJP-devices after running DEP experiments. Essentially, it has been reported that applying high voltages have destructive attributes to IJP-devices when used for DEP applications [1, 2]. The latter is caused by the flow of current – which is proportional to the applied voltage - which generates considerable amounts of heat (Joule's heating), and causes electrical stress affecting the durability, stability and robustness of traditionally fabricated [10] and thermally sintered IJP-electrodes [3, 4]. For this, we applied 5V for 15 minutes in a low conductive medium, and measured impedance readings at a frequency range between 100 Hz and 20 kHz. We noticed that the impedimetric measurements decreased by around 20% of its original value. The voltage was re-applied for an additional 15 minutes, resulting in a cumulative duration of 30 minutes, during which the impedimetric measurements remained the same, as depicted in figures S5 and S6. This confirms that the IJP-devices remain robust after being subjected to long-term, low voltage stress [5]. The obtained reduction in impedimetric values is consistent with that Rosati et al. observed upon subjecting repeated current flow to a three-layered silver-IJP electrode. The repetitive exposure to the current and voltage raised the prints' temperature and caused partial sintering of the AgNPs which in turn resulted in an increase in their admittance due to more nanoparticle coalescence [4].

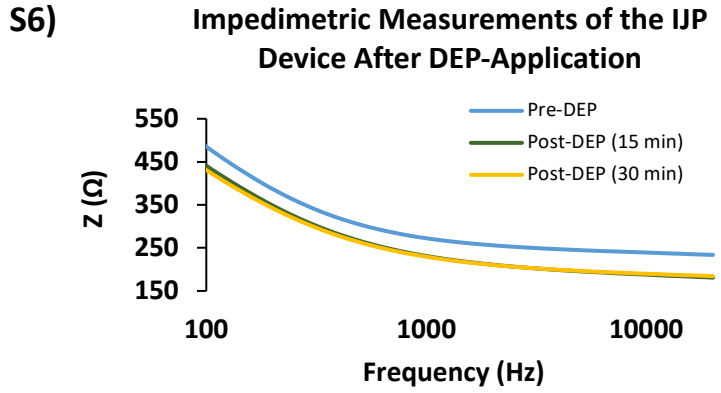

S7)

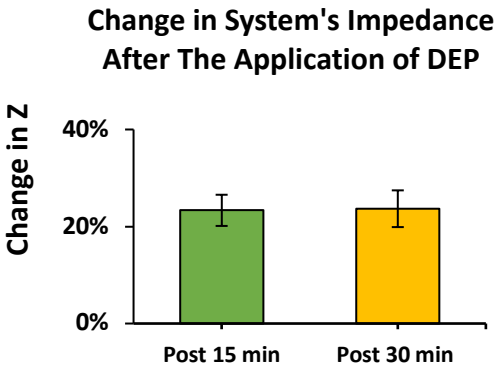
Change in System's Impedance
After The Application of DEP
Change in Z
40%
20%
0%
Post 15 min
Post 30 min

Differentiating metastatic potential of MDA-MB-231 cells via DEPIS-based sensing and enumeration

As the number of trapped cells increase due to increased cell density, ΔZ increases in all subtypes but starts to register subtle changes especially at 90,000 cell density. When comparing ΔZ at 10 kHz and 20 kHz (high frequency range), ΔZ of the three subtypes at different densities showed overlapping magnitude suggesting that our system is sensitive at low frequency rages when it comes to differentiating cells with different metastatic states (Figure S8). This is attributed to our DEPIS system's ability in detecting cellular properties at lower frequencies, which diminishes at higher frequencies [6]. In fact, at higher frequencies (>10 kHz), the system's sensitivity in detecting changes at the interface level declines since it exits the α frequency range that detects changes in electrode surface polarization and cellular membrane properties [7]. It is important to highlight that the choice of a low-conductivity medium significantly influences the efficacy of studying cancer cell behavior using EIS as opposed to higher conductive mediums [8].

When examining the impedance spectra of different cell concentrations (from 15,000 to 90,000 cells) for each subtype alone, we observe a remarkable change in the impedance and phase response, confirming our DEPIS setup is capable of enumerating different cell concentrations within the same cell subtype (Figure S9). As the concentration of the cells increases, i.e. number of trapped and captured cells increase, the amplitude of the impedance decreases while that of the phase increase as the frequency increase. This consistent drop in impedance can be attributed to the dominant role of the EDL in the low-frequency range, thereby enhancing the system's sensitivity to changes at the electrolyte-electrode interface and anticipating a rise in conductance between the electrodes [7, 9-11]. Notably, ΔZ shows an increase as we moved to higher frequencies in all cell subtype (Figure S10).

S8)

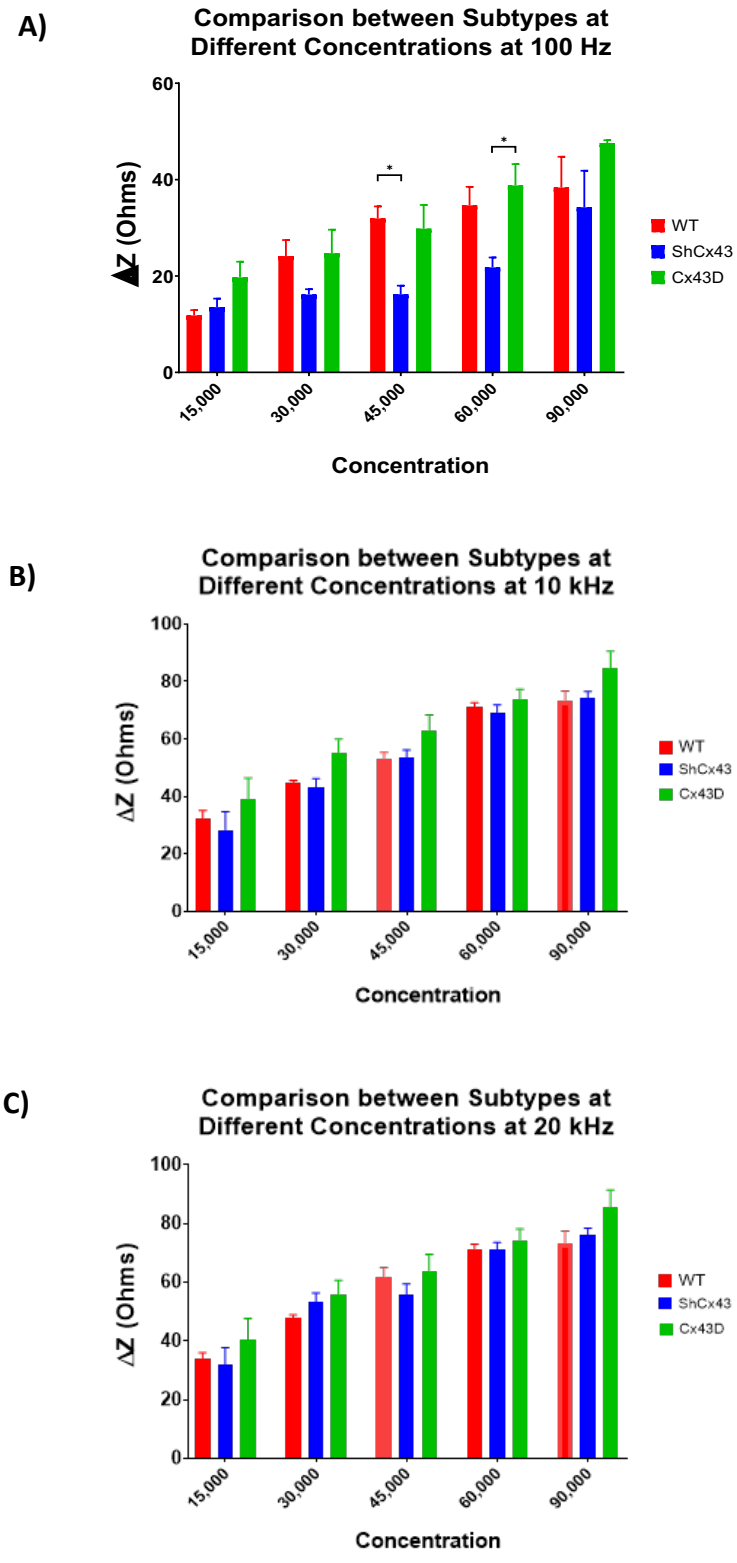

Figure S8- Difference in impedance measurements between MDA-MB-231 cell variants at a frequency of A) 100 Hz, B) 10 kHz, and D) 20 kHz. Significance reported as *, **, and *** when p-value ≤ 0.033, ≤0.002, and ≤0.001, respectively.

S9)

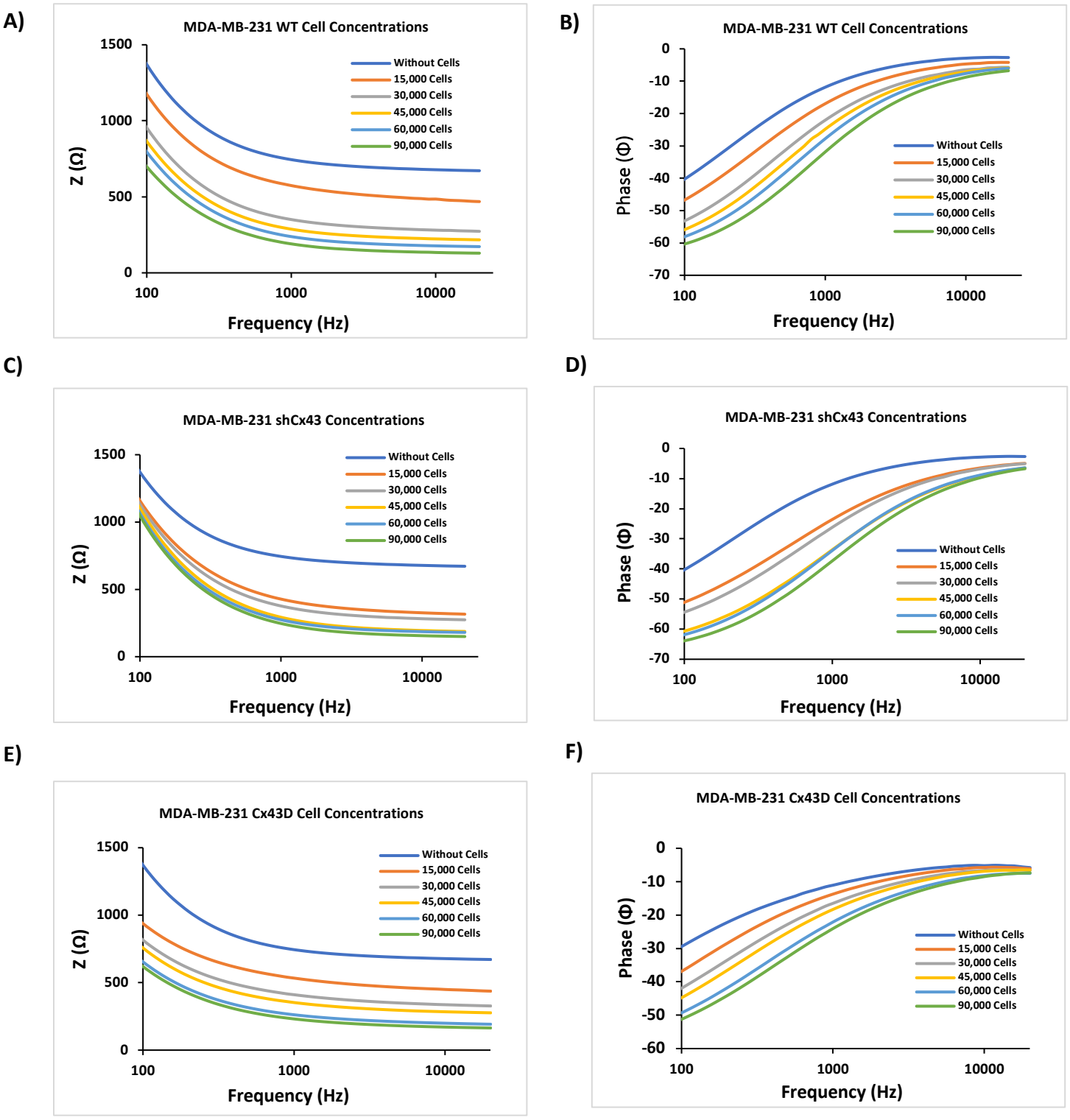

Figure S9- Impedimetric spectra (A, C, E) and phase angle (B, D, F) of MDA-MB-231 cell variants with varying cell concentrations across a frequency range of 100 Hz-20 kHz.

S10)

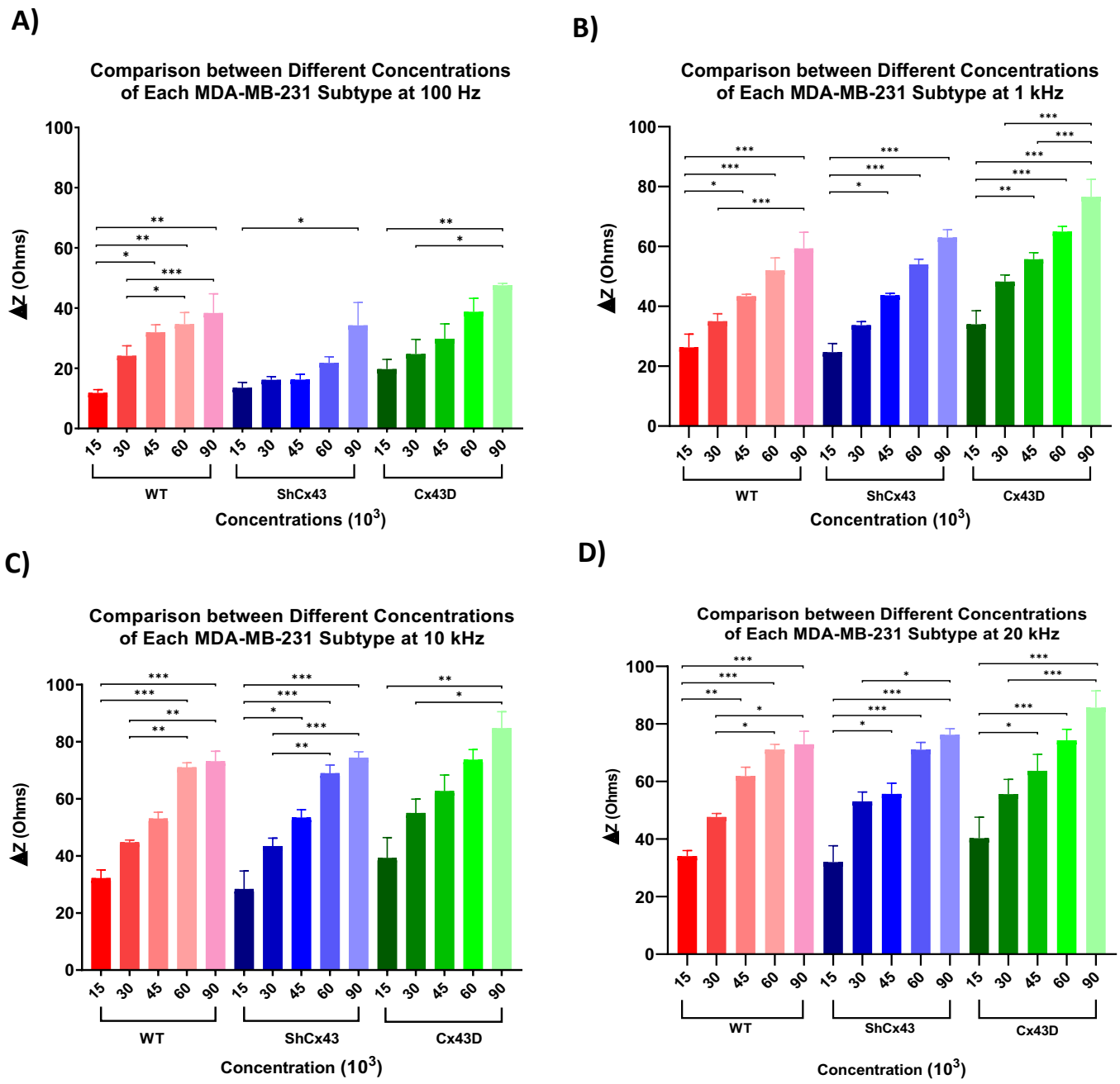

Figure-S10. Comparison between different concentrations of MDA-MB-231 WT, shCx43, and Cx43D groups at a frequency of A)100 Hz B) 1 kHz C) 10 kHz D) 20 kHz. Significance reported as *, **, and *** when p-value ≤ 0.033, ≤0.002, and ≤0.001, respectively.

Subtype	WT		shCx43		Cx43D	
Number of cells	Csol (F)	Rsol (Ω)	Csol (F)	Rsol (Ω)	Csol (F)	Rsol (Ω)
15,000	6.07E-07	451.2	6.24E-07	1.22E+03	1.05E-06	447.5
30,000	8E-07	379.6	7.44E-07	1.04E+03	1.13E-06	429.9
45,000	9.09E-07	338.1	8.07E-07	953.8	1.98E-06	424.9
60,000	9.26E-07	356.9	9.03E-07	814.3	2.03E-06	385.6
90,000	9.24E-07	336.7	9.65E-07	747	2.1E-06	374.6

Table-S1. Simulated values of the solution capacitance and resistance components in the equivalent circuit model applied with MDA-MB-231 cells with varying expressions of Cx43.

References

1. Tran, V.-T., et al., *Preparing of Interdigitated Microelectrode Arrays for AC Electrokinetic Devices Using Inkjet Printing of Silver Nanoparticles Ink.* Micromachines, 2017. **8**(4): p. 106.
2. Lee, S.H., et al., *Fabrication of a 3 dimensional dielectrophoresis electrode by a metal inkjet printing method.* Micro and Nano Systems Letters, 2013. **1**(1): p. 5.
3. Papamatthaiou, S., et al., *Ultra stable, inkjet-printed pseudo reference electrodes for lab-on-chip integrated electrochemical biosensors.* Scientific Reports, 2020. **10**(1): p. 17152.
4. Rosati, G., et al., *Silver nanoparticles inkjet-printed flexible biosensor for rapid label-free antibiotic detection in milk.* Sensors and Actuators B: Chemical, 2019. **280**: p. 280-289.
5. Valijam, S., et al., *Fabricating a dielectrophoretic microfluidic device using 3D-printed moulds and silver conductive paint.* Scientific Reports, 2023. **13**(1): p. 9560.
6. Hassan, Q., S. Ahmadi, and K.A.-O. Kerman, *Recent Advances in Monitoring Cell Behavior Using Cell-Based Impedance Spectroscopy. LID - 10.3390/mi11060590 [doi] LID - 590.* (2072-666X (Print)).
7. Daniels, J.S. and N. Pourmand, *Label-Free Impedance Biosensors: Opportunities and Challenges.* Electroanalysis, 2007. **19**(12): p. 1239-1257.
8. Crowell, L.L., et al., *Electrical Impedance Spectroscopy for Monitoring Chemoresistance of Cancer Cells. LID - 10.3390/mi11090832 [doi] LID - 832.* (2072-666X (Print)).
9. Turcan, I., et al., *Dielectrophoretic and Electrical Impedance Differentiation of Cancerous Cells Based on Biophysical Phenotype. LID - 10.3390/bios11100401 [doi] LID - 401.* (2079-6374 (Electronic)).
10. Turcan, I. and M.A. Olariu, *Dielectrophoretic Manipulation of Cancer Cells and Their Electrical Characterization.* ACS combinatorial science, 2020. **22**(11): p. 554-578.
11. Nguyen, N.-V., J.-H. Yeh, and C.-P. Jen, *A handheld electronics module for dielectrophoretic impedance measurement of cancerous cells in the microchip.* BioChip Journal, 2018. **12**(3): p. 208-215.